Pattern dynamics and competition in a photorefractive feedback system

Cornelia Denz, Michael Schwab, Markus Sedlatschek, and Theo Tschudi

Institut für Angewandte Physik, Technische Universität Darmstadt, Hochschulstrasse 6, D-64289 Darmstadt, Germany

Tokuyuki Honda

National Research Laboratory of Metrology, 1-1-4 Umezono, Tsukuba, Ibaraki 305, Japan

Received August 29, 1997; revised manuscript received January 16, 1998

We investigate the temporal dynamics of transverse optical patterns spontaneously formed in a photorefractive single-feedback system with a virtual feedback mirror. The linear stability analysis for the system is reviewed and extended to the region of larger propagation lengths. The stationary patterns obtained experimentally are classified as a function of feedback reflectivity and feedback mirror position. Inserting masks into the feedback path permits pattern selection and control by Fourier filtering. When an asymmetry that is due to noncollinear pump beams is introduced, the otherwise stationary hexagons show several complex but periodic rotationlike motions. Furthermore, the competition of hexagonal and square patterns can be observed by the appropriate choice of feedback mirror position and coupling strength. The origin of this behavior is discussed. The temporal evolution of the patterns is illustrated by a method based on unfolding the angular distribution of the spots in the far field. © 1998 Optical Society of America [S0740-3224(98)01407-6]

OCIS codes: 190.5330, 190.4420, 190.3100.

1. INTRODUCTION

Spontaneous pattern formation in nonlinear optics has recently attracted considerable interest. A generic mechanism that leads to the formation of spatial patterns is the transverse modulational instability of counterpropagating pump waves in a third-order nonlinear medium with respect to the emission of spatial sideband beams with a certain transverse wave vector. Transverse spatial structures, most of them hexagonal, have been observed in a variety of nonlinear media as such as atomic vapors,[1,2] liquid crystals,[3,4] a liquid-crystal light valve,[5] photorefractive crystals,[6] and organic films.[7] When the sidebands are emitted at an angle of 60° relative to each other in the transverse plane, the distance between two sidebands has the same magnitude as the distance between a sideband and the pump beam. Thus these sidebands are resonantly excited, giving rise to an arrangement of the sidebands in a hexagonal spot array. Vorontsov and Firth[8] explained the hexagon formation as a nonlinear interaction and mutual support of three "superactive roll solutions" with wave vectors $\mathbf{k}_i$ fulfilling the resonance condition $\mathbf{k}_1 + \mathbf{k}_2 + \mathbf{k}_3 = 0$.

In this paper our focus of interest is on the dynamic properties of the transverse patterns that are spontaneously formed in a photorefractive single-feedback system with a virtual feedback mirror. In addition to the conventional hexagonal patterns, square and squeezed hexagonal patterns were experimentally observed in this system,[9] which was to our knowledge the first experimental observation of such patterns spontaneously formed in an optical feedback system. Despite the variety of stationary patterns; in this paper we focus on the dynamic behavior of the patterns. It was shown by Honda[10] that a rotation of the far-field and a flow of the corresponding near-field hexagonal patterns in a photorefractive single-feedback system similar to the system under consideration here can be induced by transverse intensity gradients of the pump beams. Mamaev and Saffman[11] observed a more complex rocking motion of the pattern in the case of noncollinear pump beams. In this paper we present investigations of pattern dynamics that are due to two different mechanisms. An induced angular misalignment of the counterpropagating beams leads to periodic rotationlike motions, whereas the competition, i.e., the temporal alternation, of different patterns is obtained without an angular misalignment for an appropriate choice of feedback mirror position and coupling strength.

This paper is structured as follows. In Section 2 we review the linear stability analysis for the system and discuss its consequences for our particular system. The theory is shown to agree well with experimental results for pattern size and also explains the lack of pattern formation for certain positions of the virtual mirror. We performed an extension of the analysis to large propagation lengths, showing leaps of the sideband angle in that region. In Section 3 the occurrence of different types of pattern, depending on the system parameters, is experimentally investigated. The suitability of Fourier filtering in the feedback path for pattern selection and control is shown in Section 4. Because the main concern of this paper is the temporal dynamics of the patterns, we introduce an appropriate visualization method in Section 5. Pattern dynamics that are due to an induced noncollinearity of the pump beams is investigated in Section 6.

0740-3224/98/072057-08$15.00

The spontaneous competition of different patterns is investigated, and its possible origin is discussed in Section 7.

2. THEORETICAL ANALYSIS

The interaction geometry of our system is depicted schematically in Fig. 1. A plane wave of complex amplitude F is incident upon a thick photorefractive medium of length l, where it interacts with a counterpropagating feedback beam of complex amplitude B, which is provided by reflection of a forward wave F from a feedback mirror. These two beams are coupled by means of a reflection grating of wave vector $2k_0n_0$ inside the photorefractive medium, where k_0 is the vacuum wave number of beams F and B and n_0 is the linear refractive index of the photorefractive medium. In the case under consideration, a thin biconvex lens is introduced into the feedback path at distance $2f$ from the medium's back surface and a distance $2f + L$ from the feedback mirror. The lens images the mirror at a distance L from the medium's back surface and thus creates a virtual mirror near the medium, which we can move by shifting the feedback mirror. The advantage of this system compared with other feedback mirror configurations is that the virtual mirror can be placed inside the medium, allowing for negative propagation lengths. During the round trip in the feedback path the sideband beams experience a phase lag of $k_0\theta^2L$ relative to the carrier beam, where θ is the angle between the carrier and the sidebands. A negative propagation length thus corresponds to a negative phase lag.

Our linear stability analysis for obtaining the threshold condition of pattern formation in this system is based on the transverse modulational instability of two energy-exchanging counterpropagating beams, which couple through a single reflection grating (see, e.g., Refs. 12 and 13). A different approach by Kukhtarev *et al.*[14] based on pairwise two-wave mixing of the incident beam and the sidebands that are generated by scattering through transmission gratings is not considered here. In contrast to ours, that approach would require taking into account the angular dependence of the coupling coefficient γ to calculate interactions by means of several transmission gratings in different orientations. Note that, in general, the result of a linear stability analysis for a nonlinear system is limited to the calculation of the magnitude of the unstable transverse wave vector and thus the emission angle of the generated sideband beams. The formation of different pattern types in the system cannot be deduced from a linear stability analysis but requires a nonlinear analysis, which has not yet been developed for photorefractive systems.

Following the detailed treatment by Honda and Banerjee[12] for the case of a simple feedback mirror, we extended this analysis for the case of negative propagation lengths.[9] We now review this analysis, extend it to larger propagation lengths, discuss the consequences of a lower coupling strength on the occurrence of sidebands, and compare the results with experimental observations. For details and assumptions see Refs. 9 and 12.

The system under consideration is governed by the usual equations for contradirectional two-beam coupling[9]:

$$\frac{\partial F}{\partial z} - \frac{i}{2k_0n_0}\nabla_\perp^2 F = i\gamma\frac{|B|^2}{|F|^2 + |B|^2}F, \tag{1}$$

$$\frac{\partial B}{\partial z} + \frac{i}{2k_0n_0}\nabla_\perp^2 B = -i\gamma^*\frac{|F|^2}{|F|^2 + |B|^2}B, \tag{2}$$

where z is the propagation direction, $\perp$ denotes the transverse direction, and γ is the complex photorefractive coupling coefficient. The term $i/(2k_0n_0)\nabla_\perp^2$ accounts for variations in the transverse beam profile. To perform a linear stability analysis we assume that the amplitudes of the forward and the backward waves are modulated by weak sidebands according to

$$F(\mathbf{r}) = F_0(z)[1 + F_{+1}(z)\exp(i\mathbf{k}_\perp \cdot \mathbf{r}_\perp) + F_{-1}(z)\exp(-i\mathbf{k}_\perp \cdot \mathbf{r}_\perp)], \tag{3}$$

$$B(\mathbf{r}) = B_0(z)[1 + B_{+1}(z)\exp(i\mathbf{k}_\perp \cdot \mathbf{r}_\perp) + B_{-1}(z)\exp(-i\mathbf{k}_\perp \cdot \mathbf{r}_\perp)], \tag{4}$$

where $\mathbf{k}_\perp$ is the transverse wave vector of the sidebands, $\mathbf{r}_\perp$ denotes position in the transverse plane, and $F_{\pm1}$ and $B_{\pm1}$ are the relative amplitudes of the sidebands. The boundary conditions for sideband generation with a feedback mirror are

$$F_{\pm1}(0) = 0, \tag{5}$$

$$B_{\pm1}(l) = \exp(2ik_dn_0L)F_{\pm1}(l), \tag{6}$$

where $k_d \equiv k_0\theta^2/2n_0$ is the wave number corresponding to the phase lag between the carrier and the sideband per unit length in the photorefractive medium. By inserting Eqs. (3) and (4) into two-beam coupling equations (1) and (2), linearizing with respect to the amplitudes of the weak

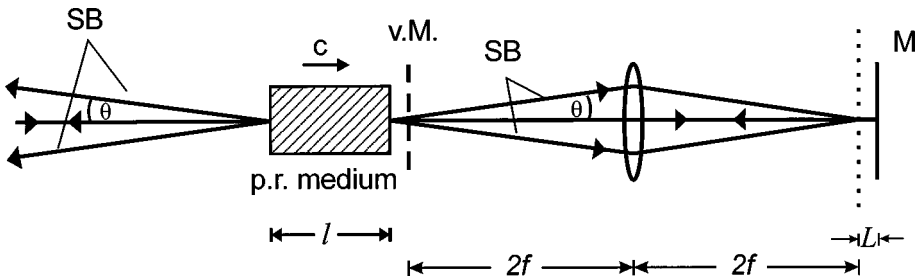

Fig. 1. Principle of the interaction geometry: SB's, spatial sidebands; M, mirror; v.M., virtual mirror; L, propagation length; l, crystal length; θ's, sideband angles; p.r., photorefractive.

sideband beams and, using boundary conditions (5) and (6), we obtain the threshold condition for sideband generation as[12]

$$\cos wl \cos k_d l + \frac{\gamma_I}{2w} \sin wl \cos k_d(l + 2n_0 L) + \frac{\gamma_R + 2k_d}{2w} \sin wl \sin k_d l - \frac{\gamma_R}{2w} \sin wl \sin k_d(l + 2n_0 L) = 0, \quad (7)$$

where γ_R and γ_I are the real and the imaginary parts, respectively, of photorefractive coupling coefficient γ and $w = ({k_d}^2 + \gamma_R k_d - {\gamma_I}^2/4)^{1/2}$. In our experiments we used $KNbO_3$ as a photorefractive medium, which shows a nonlocal photorefractive response and performs pure energy coupling between the beams. Thus we assume that $\gamma_R = 0$ in what follows.[13] For photorefractive media with local response, a detailed linear stability analysis was published recently.[15]

Threshold function (7) can be plotted to express γl as a function of $k_d l/\pi$ for various normalized propagation lengths $n_0 L/l$ (see Fig. 2 of Ref. 9 for typical examples). The angle θ of sideband emission corresponds to the value of $k_d l/\pi$ that gives a minimum threshold of γl. Then θ can be calculated from $\theta = (2k_d n_0/k_0)^{1/2}$ for each value of $n_0 L/l$. In Fig. 2, the angle of sideband generation is plotted as a function of the normalized virtual mirror position $n_0 L/l$ for a wide range of positions. Note that the sideband angle is symmetrical about the crystal center at $n_0 L/l = -0.5$ and that the plot is limited to the parameter region shown for visibility only. The sideband angle decreases for positive virtual mirror positions, corresponding to the simple mirror configuration, which has already been confirmed experimentally by Honda and Banerjee.[12] However, for larger positive values of $n_0 L/l$ the behavior changes significantly, and the sideband angle shows a sharp increase for certain large positive values of $n_0 L/l$, which has not yet been confirmed experimentally. This behavior can be explained by the particular shape of the threshold curve, which is shown in Fig. 3 for $n_0 L/l = 1.4$. For mirror positions near or in the crystal, the global minimum of the threshold curve is the first, i.e., the left, local minimum of the curve. Figure 3 represents the situation when the global minimum leaps from the first to the second local minimum, causing a leap of $\Delta\theta$ in the sideband angle. This situation corresponds to the sharp increase of θ in Fig. 2 at $n_0 L/l = 1.4$. For larger values of $n_0 L/l$ this condition is repeated, with other local minima providing the absolute minimum.

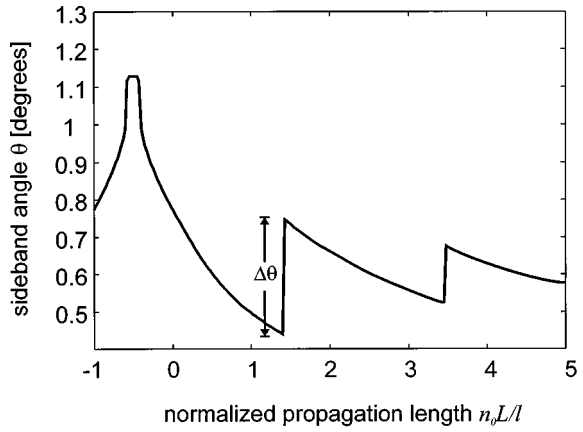

Fig. 2. Sideband angle θ as a function of normalized virtual mirror position $n_0 L/l$ according to the linear stability analysis.

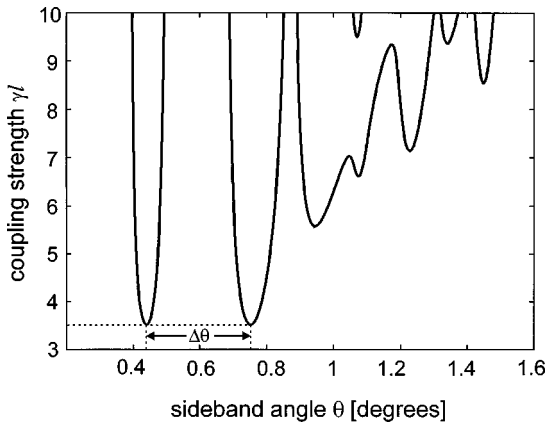

Fig. 3. Threshold curve for $n_0 L/l = 1.4$, indicating the leap in the sideband angle. The minimum of the threshold curve is passed over from the first to the second branch, resulting in a leap of $\Delta\theta$ of the sideband angle.

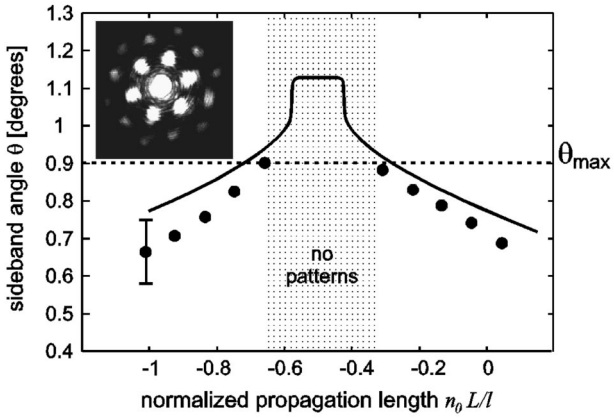

Fig. 4. Sideband angle θ as a function of virtual mirror position for the case of a virtual mirror position inside the crystal. Filled circles, experimental points; solid curve, theoretical curve. Inset, experimentally obtained hexagonal pattern in the far field, including second- and third-order spots.

In Fig. 4 the angle θ of sideband generation is plotted for $-1 \leq n_0 L/l \leq 0$ (virtual mirror inside the crystal). The filled circles indicate the sideband angles of the experimentally observed hexagonal far-field patterns. An example of such a pattern is shown in the inset of Fig. 4. To permit a theoretical investigation appropriate to experimental conditions, we shall present these experimental results in this section, whereas the experimental setup is explained in Section 3. For $-0.75 \leq n_0 L/l \leq -0.3$, no patterns were observed in the experiment, but good agreement with the theoretical pattern size is apparent for the left-hand and right-hand regions of the crystal. This lack of pattern formation in the central region can be explained if we assume that the photorefractive coupling

constant γ was too small for the generation of patterns in that region. Figure 5 shows the minima of the threshold curves as a function of the virtual mirror position. This parameter curve starts for $n_0L/l = -1$ (point A) and increases via point B ($n_0L/l = -0.7$). The turning point is point C, with a parameter value of $n_0L/l = -0.5$. Then the direction is reversed, passing point B at $n_0L/l = -0.3$ and point A at $n_0L/l = 0$ and ending at point D at $n_0L/l = 1$. If we set $\gamma l = 6$, for example, a parameter region $-0.7 \leqslant n_0L/l \leqslant -0.3$ exists, for which the threshold for sideband generation is above this value of γl. Thus pattern formation is not possible for this parameter region with the virtual mirror near the central region of the crystal. With $\theta_{max} = 0.9°$ (see Fig. 4) the estimated photorefractive coupling strength is $\gamma l = 5.5$.

3. STATIONARY PATTERNS

The experimental setup is depicted in Fig. 6. A Fe:$KNbO_3$ crystal doped with 2400 parts in 10^6 of Fe, measuring $l = 5.6$ mm along the c axis, was illuminated by a frequency-doubled Nd:YAG laser ($\lambda = 532$ nm, $P = 100$ mW), which was isolated from retroreflections by an optical diode. The crystal's c axis was chosen to be in the direction of the pump beam, leading to depletion of the input and amplification of the feedback beam. To reduce the influence of reflections from its surfaces we tilted the crystal slightly by $\approx 6°$. The beam diameter inside the crystal was approximately 350 μm, and the power incident upon the crystal was 22 mW. We chose the polarization to be in the direction of the crystal's a axis to take advantage of the large r_{13} component of the electro-optic tensor. Lens 1, with a focal length of $f = 100$ mm, was used to focus the beam into the crystal with the beam waist at its back surface. A double-passed $2f$–$2f$ imaging system ($f = 100$ mm) provided the feedback beam. Beam splitter 1 permitted observation of the feedback beam, which carried the transverse structures, and beam splitter 2 separated this beam for observation of the far-field and, by means of a Fourier-transform lens, the near-field patterns via cameras CCD 1 and CCD 2, respectively. Furthermore, beam splitter 1 permitted measurement of the input beam diameter without disturbing the feedback system.

In the inset of Fig. 4 a typical far-field hexagonal pattern is depicted that incorporates second- and third-order sidebands, whereas the corresponding near field is a honeycomb structure. The reflectivity of the optical components in the feedback path was $r = 0.95$. In this configuration with a coupling strength of $\gamma l \approx 5.5$, only patterns with hexagonal symmetry were observed. The relative intensity of the entire first-order hexagon with respect to the central spot was $\approx 12\%$ but declined for larger transverse scales to $\approx 5\%$. Note that the square and squeezed

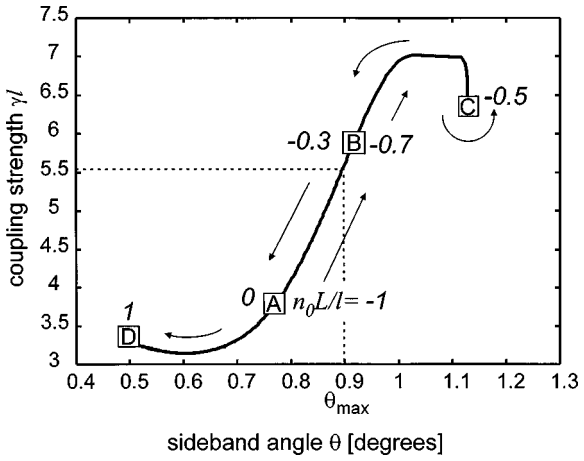

Fig. 5. Minima of threshold curves as a function of virtual mirror position for the parameter region $-1 \leqslant n_0L/l \leqslant 1$. Selected parameter values are $n_0L/l = -1, 0$ (point A), $n_0L/l = -0.7, -0.3$ (point B), $n_0L/l = -0.5$ (point C), and $n_0L/l = 1$ (point D). The largest observable sideband angle θ_{max} is indicated, corresponding to a coupling strength of $\gamma l \approx 5.5$.

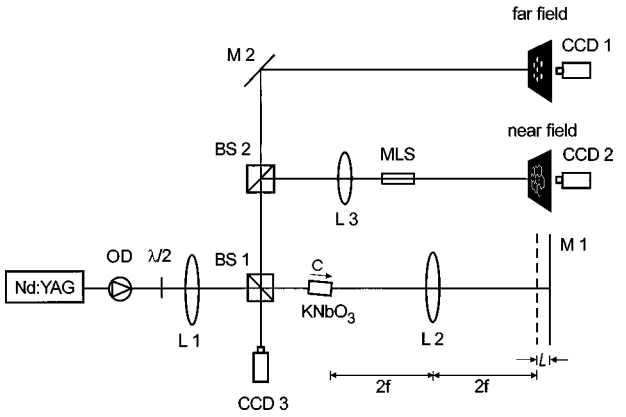

Fig. 6. Experimental setup: OD, optical diode; L's, lenses; M's, mirrors; BS's, beam splitters; MLS, microscope lens system.

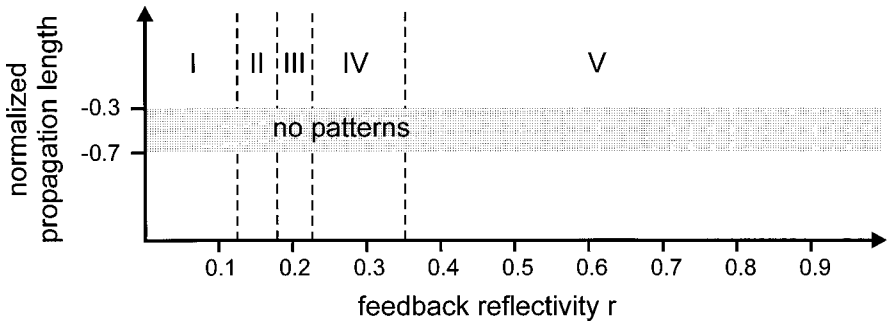

Fig. 7. Dependence of pattern type on feedback reflectivity and mirror position. I, no observable pattern; II, weak hexagonal pattern; III, pattern without geometric symmetry; IV, washed-out hexagonal pattern with emphasis on two spots opposite each other; V, static hexagonal pattern.

hexagonal patterns that we reported previously[9] were obtained for larger coupling of $\gamma l \approx 11.5$.

Reducing the feedback reflectivity by reducing the feedback mirror's reflectivity induced remarkable pattern transitions. The dependence of the pattern type on the feedback reflectivity r is shown in Fig. 7; the forbidden area, without pattern formation around the central region of the crystal, is indicated. Beginning with the unaltered high reflectivity, for feedback reflectivities $r > 0.35$ (region V), only hexagonal patterns were observed. For $0.22 < r < 0.35$ (region IV), the hexagonal pattern showed an emphasis on two spots opposite each other, although no misalignment of the pump beams was present. Introducing a small misalignment led to a competition between roll and hexagonal patterns in this region. In region III no clear pattern was observable; it is obviously a transition region between regions IV and II. In region II a hexagonal pattern was observed again, and for $r < 0.13$ (region I) no spatial sideband beams could be observed.

4. PATTERN CONTROL BY FOURIER FILTERING

Fourier filtering techniques for the manipulation of two-dimensional image information in linear optical systems are well known. Degtiarev and Vorontsov used Fourier filtering in the feedback path of a nonlinear optical liquid-crystal light-valve feedback system to suppress phase distortions.[16] Other theoretical studies have recently considered Fourier filtering techniques for the stabilization and selection of optical patterns.[17,18] A Fourier filtering method for the selection of optical patterns with the filter directly inserted into the feedback path was experimentally realized by Mamaev and Saffman.[19] Their feedback path consisted of a double-passed f–f system in which a Fourier filter plane was created in the common focal plane of the two lenses.

Without having to alter our $2f$–$2f$ feedback system we were able to realize a similar control scheme. The insertion of different spatial filters near the lens into the feedback path (where the far-field pattern was observable) altered the geometrical structure of the system in such a way that the stable hexagonal solution was suppressed and formerly underlying unstable nonhexogonal solutions of the system were excited. For a slit-shaped spatial filter, roll patterns were obtained, whereas for a cross-shaped filter square patterns were the corresponding solutions. Finally, for a large-aperture slit, squeezed hexagons were observed. It should be kept in mind that, without a spatial filter, hexagonal patterns are the only stable and thus observable solutions in this parameter region. In the case of roll and square patterns we were able to rotate the patterns continually around the central spot by slowly rotating the Fourier filter. We observed that no orientation of these patterns was favored, and thus arbitrary orientations of the patterns can be adjusted by a corresponding orientation of the Fourier filter. Roll patterns have the interesting property that the system control by the filter (i.e., the power absorbed) declines to zero in the equilibrium state. In contrast, in the case of hexagonal or square patterns higher-order spots are emitted during readout of the grating in the photorefractive medium by the forward beam and are observable at the filter. These higher-order spots are blocked by the Fourier filter, leading to small but nonzero power losses in the system for the latter case, even in the equilibrium state.

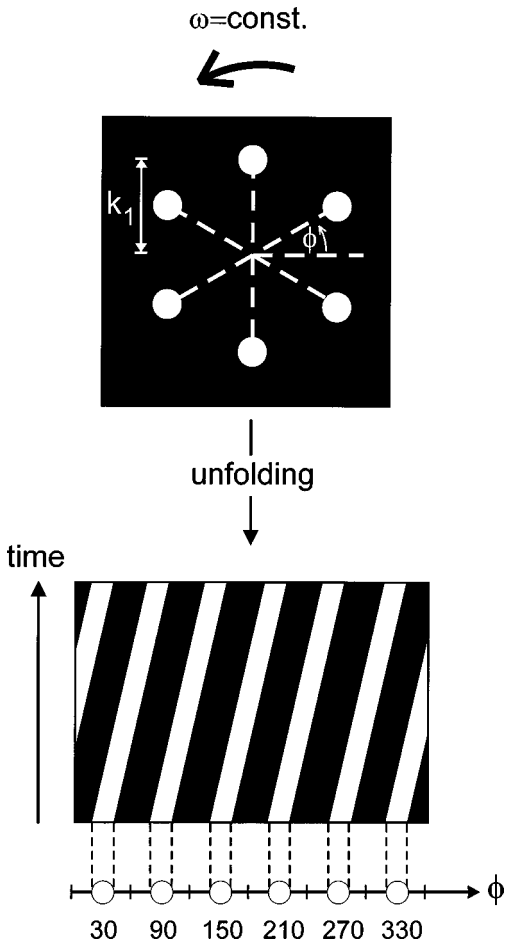

Fig. 8. Method for illustrating pattern dynamics based on the unfolding of the angular spectrum of the far-field pattern.

5. ILLUSTRATION OF PATTERN DYNAMICS

Our particular interest in the dynamics of the patterns that arise in this system requires an appropriate method for the illustration of such pattern dynamics. The most appropriate method for our purposes was proposed by Thüring *et al.*[20] Figure 8 gives a survey of this simple but effective illustration method. The distribution of far-field spots upon a circle with radius k_1 is projected upon a linear axis with the polar coordinate ϕ as the horizontal axis and time as the vertical axis. As a result, every movement of the spots on the circle leads to an appropriate pattern change in Cartesian coordinates. For example, a static hexagon causes six stripes traveling parallel in the positive y direction (time axis); a hexagon rotating with constant angular velocity ω leads to six tilted parallel stripes as shown in Fig. 8, with the slope indicating the angular velocity. The major advantage of this method is that a single image provides us with all the

information on the dynamics instead of a sequence of many single-pattern images.

6. DYNAMICS OF HEXAGONS OWING TO NONCOLLINEAR PUMP BEAMS

Shifting the lens used to focus the beam into the crystal in the transverse plane (lens L1 in Fig. 6), will induce a slight asymmetry. The counterpropagating forward and backward beams are no longer collinear and intersect at a small tilt angle. As a result, the near-field pattern starts to flow similarly to the behavior reported by Honda[10]; i.e., the honeycomb structure moves within the Gaussian beam envelope. The corresponding far-field hexagonal pattern performs a variety of different complex motions, which are the subject of investigation in this section. The situation favored for a maximum feedback reflectivity of $r = 0.95$ is depicted in Fig. 9. Two stable spots and a rotation with a fast leap back of the other four spots of the hexagon (called a rocking motion[11]) can be observed, causing us to call it rock 'n' roll motion. The axis defined by the two stable spots is always perpendicular to the lens shift and, as a consequence, to the periodic flow in the near field. As Fig. 10 indicates, the frequency of the motion depends linearly on the tilt angle introduced. This result is in agreement with previously reported experiments that used a system consisting of rubidium vapor and a feedback mirror.[21] In the special case of larger tilt angles ($>0.225°$) the rocking motion of the other four spots vanishes and a roll pattern is left in the far field. Another type of motion that can be observed in this system is a rotation of the entire hexagon, followed by a fast leap back to the initial position. This motion was observed previously in a different system and was named rocking motion.[11]

All the types of motion that we have described in this section are completely periodic in time. In the case of the rock 'n' roll motion, changes in the tilt angle result only in a change of the motion frequency, whereas for the rocking motion a slight change in the tilt angle gives rise to more-complex motions such as the one depicted in Fig. 11. The

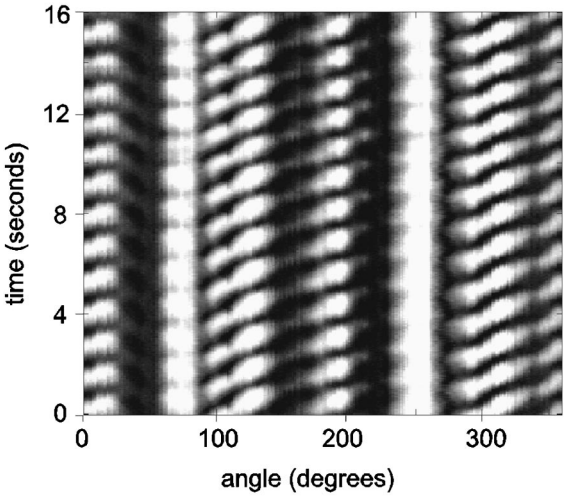

Fig. 9. Rock 'n' roll motion. Two spots, opposite each other, are nearly stable; the other four spots exhibit a rotation and a fast leap back to the initial position.

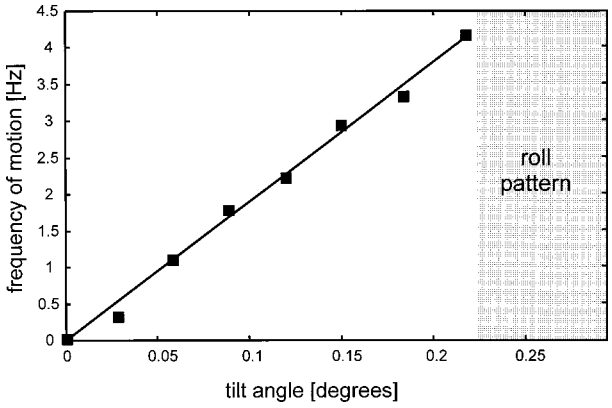

Fig. 10. Frequency of the rock 'n' roll motion as a function of the tilt angle (full angle between the incoming and the feedback beam outside the crystal).

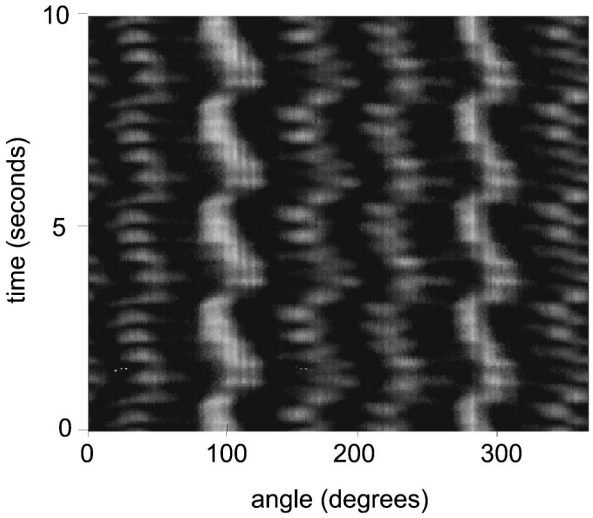

Fig. 11. Rocking motion with two time scales. All six spots show a rotation and a fast leap back on a long time scale, whereas on a shorter time scale the spots oscillate periodically.

situation shown here consists of a rocking motion with two different time scales. The regular rocking motion is evident, but all spots also oscillate periodically on a shorter time scale. Numerous other complex motions situations were also found, but they are beyond the scope of this paper. The origins of these different types of motion are currently under investigation.

When the feedback reflectivity is significantly reduced in this region of noncollinear pump beams, the temporally periodic dynamics of one pattern vanish. For $r \approx 1/3$, already a small tilt angle ($\approx 0.1°$) between the pump and the feedback beam leads to completely new behavior. In contrast to the dynamics of a single pattern, a competition between two different patterns, i.e., a hexagonal and a roll pattern, was observed, with the roll solution being preferred for larger tilt angles. The competition of different patterns without asymmetry is the subject of Section 7.

7. PATTERN COMPETITION

Besides the pattern dynamics discussed in Section 6, which are induced by noncollinear pump beams, a spon-

taneous temporal alternation of patterns of different geometries without an induced noncollinearity, a Fourier filter, or any other external inference can be observed in this system, which is due to pattern competition.[22] In the experiments reported in this section the alignment of the pump beams was controlled, and thus noncollinearity can be excluded as a possible origin of the dynamics.

We previously reported the observation of square patterns in this system for large values of the coupling strength $\gamma l \approx 11.5$ and a virtual mirror position inside the crystal.[9] Note that the pattern collapses in this region for smaller values of γl, as was discussed in the previous sections. When the virtual mirror was placed at a position between regions where stable hexagonal or square patterns were observed ($n_0 L/l \approx -0.25$; see Fig. 6 of Ref. 9), hexagonal and square patterns (shown in Fig. 12) appeared alternately in time in a nonperiodic manner.

In Fig. 13 a time sequence of such a competition is shown, illustrated by the method explained above. Because the six spots of a hexagonal pattern all lie upon a circle of a specific radius k_1 around the central spot but only four spots of the square pattern lie upon this radius (cf. Fig. 12), the competition is also shown for the four spots in the corners of the square at a distance $\sqrt{2}k_1$ from the central spot. Nevertheless, the hexagon and the square have the same transverse scale k_1. The top part of Fig. 13 shows the temporal evolution of the spots of distance k_1, and the bottom part shows the same for the spots of distance $\sqrt{2}k_1$, i.e., the corners of the square. Note that both parts of Fig. 13 refer to same time sequence of the same competition scene. Of course, only a limited excerpt of the competition can be shown in Fig. 13. It should be mentioned that different excerpts of the same competition sequence do not differ significantly. When longer time sequences of a competition sequence are looked at, it becomes more obvious that the pattern alternation during the competition is irregular in time and is thus nonperiodic.

A number of significant conclusions can be drawn from the two parts of Fig. 13. It is clearly apparent from the top part of the figure that two spots remain stable during the competition; they are in common for the hexagonal and the square patterns and are thus emphasized by the visualization method. This behavior may be due to a roll pattern coexisting with both of the temporally alternating patterns. The figure also shows that a coexistence of a hexagonal and a square pattern does not occur for a significant time interval. It is also apparent from the bottom part of Fig. 13 that the occurrence of spots with distance $\sqrt{2}k_1$ almost completely coincides with the appearance of the other four spots of the square pattern, as one can see by comparing the two parts of the figure. Furthermore, the fact that the vertical lines in Fig. 13 formed by the temporal evolution of the spots are not tilted proves that the hexagonal and the square patterns do not rotate during their existence. This result in turn confirms that an angular misalignment of the pump beams was not present and that the beams were in fact collinear.

The nonperiodic spontaneous alternation of hexagons and squares can obviously be explained in the following way. On the border between the regions for the existence of stable hexagonal and stable square solutions, both solutions are possible, and the system itself spontaneously oscillates between them.

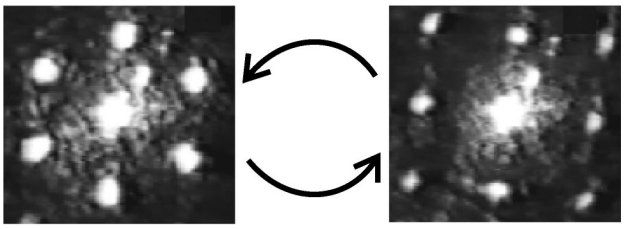

Fig. 12. Experimentally observed far-field pattern of (left) hexagonal and (right) square symmetry. For strong coupling of $\gamma l \approx 11.5$ and an appropriate choice of the virtual mirror position (e.g., $n_0 L/l \approx -0.25$), the patterns alternate in time.

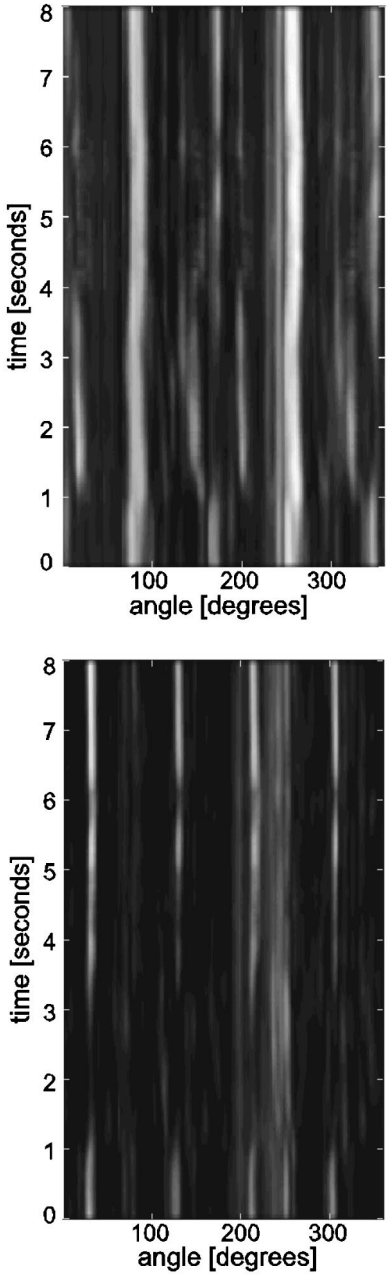

Fig. 13. Angular distribution of spots during competition of hexagons and squares. Top, radius $k = k_1$; bottom, radius $k = \sqrt{2}k_1$.

A theoretical description of this behavior should include both transverse dimensions and time. Although the treatment of this problem is extremely complicated and has not yet been fully developed, first approaches to contradirectional two-beam coupling without feedback in one transverse dimension and time have been developed.[23,24]

8. CONCLUSION

We have investigated the dynamics of patterns formed in a photorefractive single-feedback system with a virtual feedback mirror. The linear stability analysis for the system was reviewed and extended to the region of larger propagation lengths. The pattern size predicted by the theory was shown to be in good agreement with the experimental results. In addition, within the framework of linear stability analysis, we were able to explain the lack of pattern formation for certain feedback mirror positions at lower coupling strengths. The patterns that can be observed for reduced feedback reflectivities were discussed. Moreover, the possibility of controlling the type and orientation by a Fourier filter in the feedback path was shown. Complex rotationlike periodic motions of the hexagonal pattern were induced by an angular misalignment of the counterpropagating pump beams, and a linear dependence of the frequency of motion on the magnitude of the misalignment was obtained. Finally, we described the spontaneous oscillation of the system between hexagonal and square patterns.

ACKNOWLEDGMENTS

The authors acknowledge fruitful discussions with B. Thüring, R. Neubecker, and T. Rauch. This study was supported by the Deutsche Forschungsgemeinschaft, Sonderforschungsbereich 185 "Nichtlineare Dynamik."

REFERENCES

1. J. Pender and L. Hesselink, "Degenerate conical emissions in atomic-sodium vapor," J. Opt. Soc. Am. B **7**, 1361 (1990).
2. A. Petrossian, M. Pinard, A. Maître, J. Y. Courtois, and G. Grynberg, "Transverse pattern formation for counterpropagating beams in rubidium vapor," Europhys. Lett. **18**, 689 (1992).
3. R. Macdonald and H. J. Eichler, "Spontaneous optical pattern formation in a nematic liquid crystal with feedback mirror," Opt. Commun. **89**, 289 (1992).
4. M. Tamburrini, M. Bonavita, S. Wabnitz, and E. Santamato, "Hexagonally patterned beam filamentation in a thin liquid-crystal film with single feedback mirror," Opt. Lett. **18**, 855 (1993).
5. B. Thüring, R. Neubecker, and T. Tschudi, "Transverse pattern formation in an LCLV feedback system," Opt. Commun. **102**, 111 (1993).
6. T. Honda, "Hexagonal pattern formation due to counterpropagation in $KNbO_3$," Opt. Lett. **18**, 598 (1993).
7. J. Glückstad and M. Saffman, "Spontaneous pattern formation in a thin film of bacteriorhodopsin with mixed absorptive dispersive nonlinearity," Opt. Lett. **20**, 551 (1995).
8. M. A. Vorontsov and W. J. Firth, "Pattern formation and competition in nonlinear optical systems with two-dimensional feedback," Phys. Rev. A **49**, 2891 (1994).
9. T. Honda, H. Matsumoto, M. Sedlatschek, C. Denz, and T. Tschudi, "Spontaneous formation of hexagons, squares and squeezed hexagons in a photorefractive phase conjugator with virtually internal feedback mirror," Opt. Commun. **133**, 293 (1997).
10. T. Honda, "Flow and controlled rotation of spontaneous optical hexagon in $KNbO_3$," Opt. Lett. **20**, 851 (1995).
11. A. V. Mamaev and M. Saffman, "Modulational instability and pattern formation in the field of noncollinear pump beams," Opt. Lett. **22**, 283 (1997).
12. T. Honda and P. P. Banerjee, "Threshold for spontaneous pattern formation in reflection-grating-dominated photorefractive media with mirror feedback," Opt. Lett. **21**, 779 (1996).
13. M. Saffman, A. A. Zozulya, and D. Z. Anderson, "Transverse instability of energy-exchanging counterpropagating waves in photorefractive media," J. Opt. Soc. Am. B **11**, 1409 (1994).
14. N. V. Kukhtarev, T. Kukhtareva, H. J. Caulfield, P. P. Banerjee, H. L. Yu, and L. Hesselink, "Broadband dynamic, holographically self-recorded, and static hexagonal scattering patterns in photorefractive $KNbO_3$:Fe," Opt. Eng. **34**, 2261 (1995).
15. A. I. Chernykh, B. I. Sturman, M. Aguilar, and F. Agulló-López, "Threshold for pattern formation in a medium with a local photorefractive response," J. Opt. Soc. Am. B **14**, 1754 (1997).
16. E. V. Degtiarev and M. A. Vorontsov, "Spatial filtering in nonlinear two-dimensional feedback systems: phase-distortion suppression," J. Opt. Soc. Am. B **12**, 1238 (1995).
17. R. Martin, A. J. Scroggie, G.-L. Oppo, and W. J. Firth, "Stabilization, selection, and tracking of unstable patterns by Fourier space techniques," Phys. Rev. Lett. **77**, 4007 (1996).
18. R. Martin, G.-L. Oppo, G. K. Harkness, A. J. Scroggie, and W. J. Firth, "Controlling pattern formation and spatiotemporal disorder in nonlinear optics," Opt. Expr. **1**, 39 (1997).
19. A. V. Mamaev and M. Saffman, "Selection of optical patterns by Fourier filtering," presented at the Topical Meeting on Photorefractive Materials, Effects and Devices, Cosponsored by the Optical Society of Japan and the Optical Society of America, June 11–13, 1997, Chiba, Japan.
20. B. Thüring, A. Schreiber, M. Kreuzer, and T. Tschudi, "Spatio-temporal dynamics due to competing spatial instabilities in a coupled LCLV feedback system," Physica D **96**, 282 (1996).
21. A. Petrossian, L. Dambly, and G. Grynberg, "Drift instability for a laser beam transmitted through a rubidium cell with feedback mirror," Europhys. Lett. **29**, 209 (1995).
22. M. Sedlatschek, C. Denz, M. Schwab, B. Thüring, T. Tschudi, and T. Honda, "Dynamics, symmetries and competition in hexagonal and square pattern formation in a photorefractive single-feedback system," presented at the Topical Meeting on Photorefractive Materials, Effects and Devices, Cosponsored by the Optical Society of Japan and the Optical Society of America, June 11–13, 1997, Chiba, Japan.
23. O. Sandfuchs, J. Leonardy, F. Kaiser, and M. R. Belić, "Transverse instabilities in photorefractive counterpropagating two-wave mixing," Opt. Lett. **22**, 498 (1997).
24. O. Sandfuchs, F. Kaiser, and M. R. Belić, "Spatiotemporal pattern formation in counterpropagating two-wave mixing with an externally applied field," J. Opt. Soc. Am. B **15**, 2070 (1998).